Thermal characterization and cost analysis of cement-based composite materials for thermochemical energy storage

Journal of Energy Storage 93 (2024) 112308

Contents lists available at ScienceDirect

Journal of Energy Storage

journal homepage: www.elsevier.com/locate/est

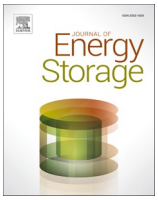

Research papers

Thermal characterization and cost analysis of cement-based composite materials for thermochemical energy storage

Simone Salustro [a,b], Luca Lavagna [a,*], Vito Fernicola [c], Denis Smorgon [c], Alessio Mondello [d], Eliodoro Chiavazzo [d,*], Matteo Pavese [a]

[a] Department of Applied Science and Technology, Politecnico di Torino, Corso Duca degli Abruzzi 24, 10129 Torino, Italy
[b] Cismondi Srl, Via Borgo Sant'Anna 28/A, 12100 Cuneo, Italy
[c] Istituto Nazionale di Ricerca Metrologica, Strada delle Cacce 91, 10135 Torino, Italy
[d] Department of Energy, Politecnico di Torino, Corso Duca degli Abruzzi 24, 10129 Torino, Italy

ARTICLE INFO

Keywords:
Thermal energy storage
Cement composite
Sorbent material
Seasonal energy storage
Energy analysis

ABSTRACT

The objective of this study is the synthesis and thermal characterization of cement-based composites for thermochemical energy storage (TES), focusing on three cement families: Portland Cement (PC), Calcium Aluminate Cement (CAC), and Calcium Sulfoaluminate Cement (CSA). We explore the potential of those composites in enhancing energy storage capabilities, while being cost-effective and robust. The research has involved composites with varying proportions of sepiolite to enhance porosity and reduce costs. An in-situ synthesis technique was conveniently employed allowing promising results on control over salt content. Water vapor-sorption analyses were conducted on six selected samples at two temperatures (30 °C and 50 °C) and across five relative humidity points. The Polanyi adsorption potential theory was employed to extend the analysis and model realistic operating cycles. We found that the top-performing composite exhibited an energy density of 85 MJ/m^3 with a storage cost of 9.30 €/kWh, thus resulting comparable or superior to materials like Zeolite 13×/$MgSO_4$ and silica gel/$CaCl_2$, but lower than vermiculite/$CaCl_2$ or LiCl. Nonetheless, the novel composites demonstrate lower costs and promising behavior with respect to important challenges as deliquescence or poor mass transport. The synthesized cement-based composites show significant potential in TES technology, though further optimization is still requited in terms of energy density and material cost. This research also suggests that cost reductions for CAC and CSA cements through scale economies and material mixing strategies, like combining CAC with PC might be feasible to further enhance the viability of these composites in TES applications.

1. Introduction

Sorption thermal energy storage (STES) belongs to the broader family of thermo-chemical energy storage, with which it shares the basic operating principle of exploiting a reversible physical or chemical reaction to store and release heat. A definitive taxonomy of this broad branch of TES systems has not been established yet [1]. Coined by McBain in 1909 [2], the term 'sorption' is used to describe both adsorption and absorption phenomena, in which the first refers to the attachment of a gaseous or liquid specie (adsorbate or sorbate) on the surface of a solid (adsorbent or sorbent), while the latter is a volumetric phenomenon in which the absorbate is incorporated within the bulk structure of the absorbent, typically a liquid, even modifying it. With respect to the broader thermochemical energy storage, STES are generally considered for the storage and use of low temperature heat. Among other applications, this may pave the way to affordable seasonal thermal energy storage for residential space heating, by harvesting solar thermal energy through solar collectors or concentrating solar power in the temperature range between 90 °C and 150 °C [3] for a later use in winter time.

Yu et al. [4] proposed a classification of STES based on the materials involved which, in turn, characterize the type of forces, reactions and energies at stake. They divided STES in:

- Liquid absorption, widely used for absorption chillers and heat pumps (liquid salt solutions) and in industrial refrigeration (ammonia-water), have gained much attention for TES applications

* Corresponding authors.
E-mail addresses: luca.lavagna@polito.it (L. Lavagna), eliodoro.chiavazzo@polito.it (E. Chiavazzo).

https://doi.org/10.1016/j.est.2024.112308
Received 31 August 2023; Received in revised form 29 April 2024; Accepted 24 May 2024
Available online 30 May 2024

as well, in which the most popular aqueous solutions are those based on LiBr and on NaOH [5].

- Solid adsorption, based on physical surface interactions between a solid adsorbate and a gaseous adsorbate. The latter is generally constituted by water vapor, although also methanol and ammonia have been studied. Adsorbates to investigate are selected between porous materials characterized by a high specific surface, in order to guarantee a large sorbate hosting capability; the most common are zeolites, activated carbon, natural rock, silica gel and metal organic frameworks (MOFs) [6,7].
- Chemical reaction, which for solar TES applications mainly involve hydration/dehydration reactions of hygroscopic salts with water vapor. In general, due to stronger binding energy in chemical interaction as compared to solid adsorption, this implies higher energy densities (e.g. 2.8 GJ/m^3 in the case of the full hydration of $MgSO_4$ [8]) but also higher desorption temperatures. However, even if several salts exist that could be used [9], most of them unfortunately present important limitations [10]. The use of pure hygroscopic salts in bulk, indeed, often exposes them to the phenomenon of deliquescence and degradation, which seriously affects the materials stability and storage performance after some cycles [1]. Furthermore, those salts are generally characterized by a low heat conductivity (0.4–1 W/m K), hindering the heat transfer needed in any heat-based process. Their use in bulk also sensibly hampers the mass transport, necessary in any STES to allow the sorbate (typically water vapor) to easily reach adsorbent sites [1].

Physically porous sorbents (zeolite, silica gel etc.) are attractive for stable performances but have low energy density and energy capacity. Chemical sorbents are characterized by higher storage capacities, although the phenomenon of deliquescence, which may affect grain stability, limits their performance. Recently, several studies proposed a family of new solid sorbents, consisting of "*hygroscopic salts inside a porous matrix with open pores*" (CSPM) [11]. Indeed, the presence of the porous matrix can help alleviating salt deliquescence and degradation, but also significantly improve the mass and heat transfer phenomena, e.g. through a typically higher heat conductivity of the matrix materials with respect to the salts as well as a much more efficient sorbate mass transfer. Moreover, being composites, their properties may be tailored more accurately for given applications [12]. As such, CSPM are considered among the most promising class of materials for solar driven STES and are gaining a relevant increase of attention in the scientific literature [13–16].

In a work of 2011, Hongois and coworkers [17] analyzed a zeolite 13× loaded with a 15 % in weight of $MgSO_4$ adsorbing moist air from buildings, and a temperature lift of 30 °C was measured. By means of a differential scanning calorimetry (DSC), the composite behaved similarly to pure zeolite 13× but with higher peaks at maximum temperature. Because of this, the researchers assumed that $MgSO_4$ can exchange ions with the very zeolite structure and does not behave as a mere salt confining host matrix. The energy density of 0.6 GJ/m^3 was thus evaluated, 27 % more than the zeolite theoretical one of 0.47 GJ/m^3. In 2013 Lele and colleagues [18] studied thermal conductivity of pure $CaCl_2$ and composites with silica gel or vermiculite, finding a value of 0.39 W/(m K) for pure calcium chloride and 0.83 W/(m K) for silica gel composites and 0.74 W/(m K) for vermiculite composites, proving the thermal conductivity improvement of composite materials. In their work of 2014, Casey and coworkers [19] investigated three different salts, namely $CaCl_2$, $MgSO_4$ and LiBr, as active materials for composites with silica gel, zeolite 13× and vermiculite as host matrices. While matrices were characterized by Type I adsorption isotherms, all the composites have shown a Type IV isotherms with hysteresis loops. The observed peculiar behavior appears linked to structural damage induced by the presence of salt to both zeolite 13× and, to a lesser extent, silica gel host matrices. In particular, the former has shown a wider pore size distribution with respect to the narrow one observed for the pure matrix. Because of this, composites based on silica gel and zeolites were able to adsorb less water vapor. Conversely, the structure of vermiculite remained unchanged. In the study, composites containing $CaCl_2$ and LiBr exhibited the highest energy density values: specifically, 0.18 GJ/m^3 for $CaCl_2$ and 0.17 GJ/m^3 for LiBr, with salt contents reaching 56 % and 65 % respectively. However, the above energy density values are far from the one obtained by Hongois et al. in 2011 [17]. Again in 2014, Druske and coworkers [20] studied carbon foams and expanded natural graphite as host matrices and impregnated them with KCl and $CaCl_2$, addressing the deliquescence issue of chlorides. Composites improved both thermal conductivity and water uptake of pure salts. The most interesting results were provided by the couple expanded natural graphite/$CaCl_2$, which has shown a water uptake of 0.45 g/g, a thermal conductivity between 0.74 and 1.64 W/m K and an energy density of 0.63 GJ/m^3. In recent years, other potential porous matrices have also been under study. Anodic Aluminum Oxides (AAO) are emerging as possible host matrices for hygroscopic salts. In 2020, Yilmaz and coworkers investigated AAO impregnated with various inorganic salts ($LiCl_3$, $LiNO_3$, $MgCl_2$, $CaCl_2$) either individually or in multiple combinations. The maximum energy density achieved was 461.8 kJ/kg using an AAO impregnated with a binary mixture (1:1) of LiCl and $LiNO_3$ [21], which is lower than the energy density of the vermiculite-LiCl composite (1147.5 kJ/kg) [22]. Additionally, metal-organic frameworks (MOFs) have been tested as matrices for CSPM materials. In 2019, D'Ans and colleagues [23] obtained an energy density of 233 kWh/m^3 for $SrBr_2$ encapsulated in a MOF structure, with a dehydration temperature of 80 °C.

A brief survey on the latest advancements in this field was provided by four reviews [15,24–26] that cover all the aspects related these topic.

Despite these premises, the performances in terms of energy densities provided by a large number of composite materials are currently not considerably different with respect to the ones provided by pure adsorbents such as zeolite 13× [27]. However, although zeolite 13× is one of the most common materials for water sorption heat storage, its cost and desorption temperature are too high to allow its actual adoption as heat storage means, especially for seasonal storage [28].

The aim of this work is to synthesize and study an innovative composite material for seasonal low-temperature sorption heat storage. Particular attention is focused on the composite affordability and widespread availability, in order to possibly contribute to develop new sorbent material that can be commercially attractive in the near future, even at the expense of smaller energy density values. For this purpose, cement will be investigated as a potential host matrix for various salt hydrates. In fact, dry cement paste is a porous material, cheap and widely used on a global scale, having undergone extensive economies of scale. In addition, its porosity can be controlled rather easily by acting on the water to cement ratio, a key parameter involved in the cement paste synthesis, and by adding a second porous phase, which in this case is sepiolite. Characterization of pure cement paste properties, synthesis and analysis of cement-based composites materials, potential water sorption heat storage applications for space-heating and economic analysis will be provided and discussed in this work. The cycle conditions used in this work are illustrative and have been chosen primarily to facilitate comparison among different materials. However, we can consider these conditions realistic for a geographical area like southern Italy.

1.1. Materials

In this work Ultracem 52,5 R and Ali Pre Green both from Italcementi has been chosen as Portland cement (PC) and Calcium Sulfo Aluminate (CSA) cement, respectively. For Calcium Aluminate Cement (CAC) the Ciment Fondu® from Imerys Aluminates has been selected. In order to improve the porosity of the dry cement paste a second porous phase has been introduced therein, namely sepiolite from Lampa Accessories. $MgSO_4{\cdot}7H_2O$ was purchased from Merck.

2. Methods

The production of pure cement samples took place by following the typical procedure for such materials, analogous for the three types of cements: a proper amount of deionized water is mixed with a respective amount of cement powder. These amounts are chosen based on the weight ratio between water and cement, identified by the so-called w/c ratio Since the latter strongly influences the porosity of the product, different samples were produced by varying this ratio above the ones typically used for structural applications, with the aim to maximize samples porosity. When applied in the construction field, typical values of w/c for PC are 0.35–0.6 [29], while for CACs for structural applications the maximum w/c is around 0.40. Finally, CSAs are manufactured with a w/c in the range 0.5–0.6, though this depends on their specific composition. In order to increase the porosity of the samples, sepiolite was also added to the cement powder, with sepiolite/cement weight ratios up to 70 %. It should be pointed out that the water-to-cement ratio considered here is the "theoretical" one, namely the one that was employed during the production. However, not all the water might end up in the cement paste, if the phenomenon of bleeding occurs [30]. During bleeding some water separates from the paste rising to the top of the mold and is not included in the final specimen which, as a result, is thinner than the original paste level. We used the "effective w/c" ratio to represent the water that is actually included in the final sample, obtained by subtracting the bled water from the "theoretical w/c".

To produce the samples, the proper amounts of cement, sepiolite and water were blended in a beaker through a mechanical stirrer to form a homogeneous slurry which was then poured into metallic molds. Each of these molds have four compartments, allowing to simultaneously produce four specimens of the same size, with the same mix and in the same conditions. The compartments measure 80 × 20 × 20 mm, thus their available volume is 32 cm^3 and that of the entire mold is V = 128 cm^3.

Following the methodology used in a previous research [29], two types of sample preparation were performed. In the standard one (called "two-step") the cement samples were prepared with deionized water and then they were infiltrated with a saturated solution of $MgSO_4$ in order to completely fill their open porosity. Then the water was removed by heat treatment at 140 °C with the precipitation of the salt inside the pores. However, most of the best samples were obtained by an innovative methodology [25] (called "one-step") where cement was not prepared with pure water but with a saturated solution of $MgSO_4$. In this case a single preparation step is needed, and the salt results very well dispersed in the cement matrix.

After a first fast screening of several compositions following the preliminary calorimetric analysis described in the article of Lavagna et al. [29] based on PC, CAC, CSA, and their mixtures, following both two-step and one-step preparation approaches, the best materials were selected for a complete characterization. The mix proportion of these samples are reported in Table 1. In Fig. 1 samples are shown as extracted from the mold and in pelletized form, during the testing in the climatic chamber.

Table 1
Mix proportion of prepared sample.

Sample name	PC (g)	CAC (g)	CSA (g)	Water (g)	Sepiolite (g)	$MgSO_4$ (g)
CSA-S			65.21	98.00	46.00	
CSA-S-1s			65.27	61.00	46.21	34.69
CAC-S-1s		66.04		61.03	46.00	34.67
CAC-S-2s		66.29		46.02 + 61.21[a]	46.02	34.76
PCAC-S-1s-A	10.15	56.38		102.29	46.32	35.75
PCAC-S-1s-B	15.10	51.55		100.24	46.33	35.16

[a] 46.02 g is the mass of water used for sample preparation, while 61.21 g is mass of the saturated $MgSO_4$ solution used to impregnate the prepared sample.

Geometrical density was evaluated with a Radwag laboratory scale PS 510/C/1 (resolution of 1 mg), while the sample size was measured by means of a Preciva digital caliper (resolution of 0.01 mm). Being a specimen approximately 80 mm × 20 mm × 20 mm, three measurements along each side were taken and averaged to estimate its volume. Once the mass and volume of the samples was measured, their geometrical density was calculated by their ratio.

In order to study the sorption behavior and expected energy storage capabilities of the selected materials, two adsorption isotherms at two different temperatures were measured. All samples were inserted in the chamber of a 2P-2T relative humidity (RH) generator model Thunder Scientific 2500 used as primary standard for RH measurements at INRIM. The expanded uncertainties of the applied conditions were estimated to be between 0.2 %rh and 2 %rh for RH and 0.4 °C for air temperature in the test volume. An adsorption isotherm was obtained by weighing the water uptake of the samples at constant temperature under different levels of relative humidity, with a Sartorious MA-150 scale. The two selected temperatures were 30 °C and 50 °C and each isotherm has been approximated by the measured values at five different levels of RH, as a compromise between the sampling completeness of the resulting curves and the duration of the experiment. Specifically, those sampling points corresponds to 10 %rh, 30 %rh, 50 %rh, 70 %rh and 90 %rh. Additionally, a 0 %rh point was obtained by weighing the dried samples. From the experimental point of view, about 30 g of each of the 6 dry samples were weighed and hosted in aluminum disposable sample pans of 90 mm diameter and 2.50 g mass. All the pans were then placed inside the RH generator chamber at $T = 30$ °C and 10 %rh. In addition to the built-in pressure and temperature sensors of the system, two more RH sensors were placed inside the chamber to confirm the measurements. Followingly, after 24 to 36 h in the RH generator chamber, each sample was removed from it and quickly weighed (each sample was back in the chamber within 30 s) in order to reduce any spurious adsorption/desorption process due to the abrupt change of temperature and relative humidity. Once the weighing process was completed, the RH setpoint was increased to the next point and the procedure was repeated.

All the acquired mass measurements data are reported in Table S1. After the weighing process for the last point at 90 %rh of the first isotherm at $T = 30$ °C is completed, by means of an infrared thermal balance, all the samples were quickly dried back to weight values close to those observed at the beginning of the first measurement (0.12 g difference at the most for samples 8 and 9, as can be observed among the data reported in the first column in Table S1).

3. Results

According to the IUPAC classification [31] of adsorption isotherms, the plotting of the data reported in Table S1 produces curves belonging to the Type II family, as shown in Figs. 2 and 3 for the data at 30 °C and 50 °C, respectively. Type II isotherm indicates an indefinite multi-layer adsorption after the completion of the first monolayer; it is typical of adsorbent with a wide porous size distribution and associated to the presence of macropores.

These isotherms can be conveniently described through the theoretical framework developed by S. Brunauer, P. H. Emmett and E. Teller in 1938 [32], the so-called BET model. All the curves reported in the figures clearly show three different trends as a function of the RH value: below 10 %rh, between 10 %rh and 50 %rh, above 50 %rh. Starting from the first and lowest range of RH among those listed, the BET theory identifies the observed "knee" of these isotherms with the point corresponding to the completion of the monolayer coverage, in which each adsorption site is formally occupied by one water molecule. Beyond this value of RH, a rather linear trend associated with the multilayer behavior starts. Finally, once RH reaches the 50 %rh, the steepness increases due to the occurring capillary condensation in the pore cores

Fig. 1. Samples of CAC-s-1s as obtained from the mold (left) and various cement samples in pelletized form during the testing in a climatic chamber (right).

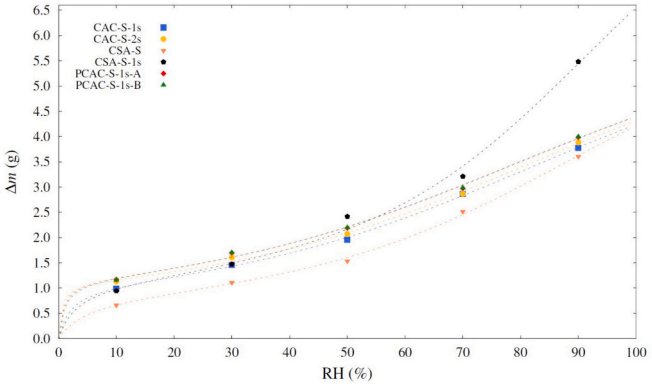

Fig. 2. Adsorption isotherms at $T = 30$ °C of the 6 samples. The curve fitting result of the experimental data through Eq. (2) is reported as well.

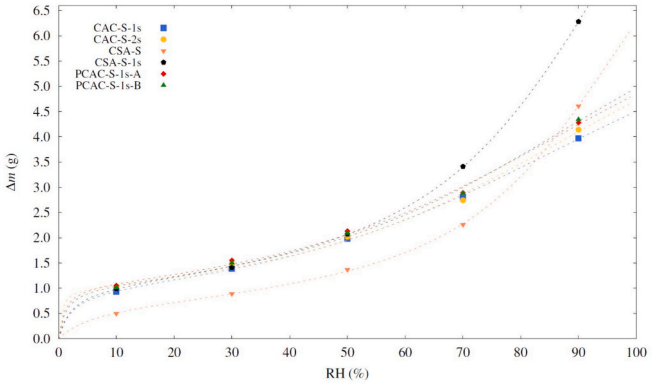

Fig. 3. Adsorption isotherms at $T = 50$ °C of the 6 samples. The curve fitting result of the experimental data through Eq. (2) is reported as well.

[33]. In their work from 1938 [32], Brunauer, Emmett and Teller proposed the following 2 models to fit the experimental data, a 2-parameters equation and a 3-parameters equation, respectively:

$$\Delta m = \frac{M_m \bullet C \bullet RH}{(1 - RH) \bullet (1 + (C - 1) \bullet RH)} \tag{1}$$

$$\Delta m = \frac{M_m \bullet C \bullet RH}{(1 - RH)} \bullet \frac{1 - (L + 1) \bullet RH^L + L \bullet RH^{L+1}}{1 + (C - 1) \bullet RH - C \bullet RH^{L+1}} \tag{2}$$

where M_m, C and L are the best-fitting parameters. Such parameters can be associated to as many physical quantities, in particular:

- M_m, is the amount of adsorbed water that corresponds to the abovementioned monolayer completion.
- C is a dimensionless quantity that suggests the interaction strength between water and sorbent and characterizes the shape of the knee, sharper for $C > 2$ or absent for $0 < C < 2$.
- L is the average number of adsorbed layers.

According to their paper [32], Eq. (1) is suitable only for experimental data in the range 5 %rh < rh < 35 %rh, while Eq. (2) can be applied in principle to the entire range of rh values. For this reason, the fitting curves shown in Figs. 2 and 3 are obtained with the three-parameters Eq. (2). The results of the various fitting process via a Levenberg-Marquardt nonlinear least-squares (NLLS) algorithm are reported in Table S2.

4. Discussion

In order to estimate the most relevant figures of merit for TES sorption applications associated to the novel synthesized materials, it is important to compute the expected cycled heat (Q_u) and energy density (E_d) under reasonable operating conditions of the TES plant.

The cycled heat, Q_u (in MJ/kg), and energy density, E_d (in MJ/m^3), are related to the amount of energy - under prescribed conditions - that the material is capable to store per unit of mass and of volume after an entire energy storage cycle, respectively. In addition to the sorbent-sorbate pair characteristics, values of these quantities are strictly related to type of STES plant, as well as to the operating and environmental temperatures. Hence, in our computations below, we will assume a water sorption closed system, charged by concentrated solar power systems operating at 140–150 °C. The above is conveniently accomplished by resorting to the typical representation of an ideal sorption-based thermal energy storage cycle (i.e. two isosteric + 2 isobaric transformation) within the Clapeyron chart. To this end an estimate of the isosteric field is necessary and can be obtained starting from the measurements of various equilibrium adsorption isotherms spanning between the two extreme temperatures, namely:

i. The user-operating temperature (here a floor heating system working at 40 °C).
ii. The thermal solar collector maximum temperature (here assumed in the order of 140–150 °C).

As only two adsorption isotherms were obtained, at 30 °C and at 50 °C, in this work the Polanyi potential theory was applied to properly scale the measured data to the other needed isotherms values.

The potential theory of Polanyi assumes the adsorption process similar to condensation, where the adsorbate particles behave like a fluid, and states the principle of temperature invariance, from which it postulates a one-to-one correspondence between the adsorption uptake

and the adsorption potential [34]. The validity of the Polanyi theory for the working pair water and sorbent materials proposed in this work, can be appreciated in Fig. 4.

By adopting a thermodynamic perspective, Polanyi, Dubinin and colleagues expressed the potential function as [35]:

$$A_{Dub} = RTln\left(\frac{p_0}{p}\right) = -RTln(RH) \quad (3)$$

This allows to express the adsorbed load Δx_i (i.e. the data reported in Table S1 normalized on the mass initial value):

$$\Delta x_i = \frac{m_i - m_0}{m_0} \quad (4)$$

as a function of this potential only, instead of considering the two parameters p and T [34], or rather

$$\Delta x \propto f(A_{Dub}) \quad (5)$$

In principle thus it is possible, by plotting the experimentally obtained load on a $A_{Dub} - \Delta x$ graph, to obtain a single "*characteristic curve*" irrespective of the temperatures and pressures used. Table S3 collects the adsorbed load, defined according to Eq. (4), for all the 6 investigated samples together with the corresponding adsorption potential value described in Eq. (3). When plotted, the experimental data collected in this table return the trends reported in Fig. 4: black squares refer to the data obtained from the 30 °C isotherm, while blue circles refer to the data from the 50 °C-isotherm. As can be observed, generally the 30 °C data show higher values of adsorbed load (Δx_i) than that of the 50 °C-data, which is in line with what expected since adsorption from gas phase is favored by low temperatures. This is in line with all the plotted data except for one, namely that reported with a red square in both Fig. 4 and Table S3, which corresponds to the 90 %rh for the 30 °C-isotherm. For all the 6 samples, this value appears well below the expected value, namely above the 90 %rh for the 50 °C-isotherm.

The point in question, according to the literature [36], would correspond to the salt deliquescence threshold. Nevertheless, during the tests, we did not observe salt deliquescence outside the matrix. Most likely, we hypothesize that this point could be attributed to a lack of adsorption equilibrium in that condition and therefore the samples needed a further stay in the climatic chamber.

As can be observed in Fig. 4, all the experimental data for the 6 investigated samples origin rather evident trends, with the exception of

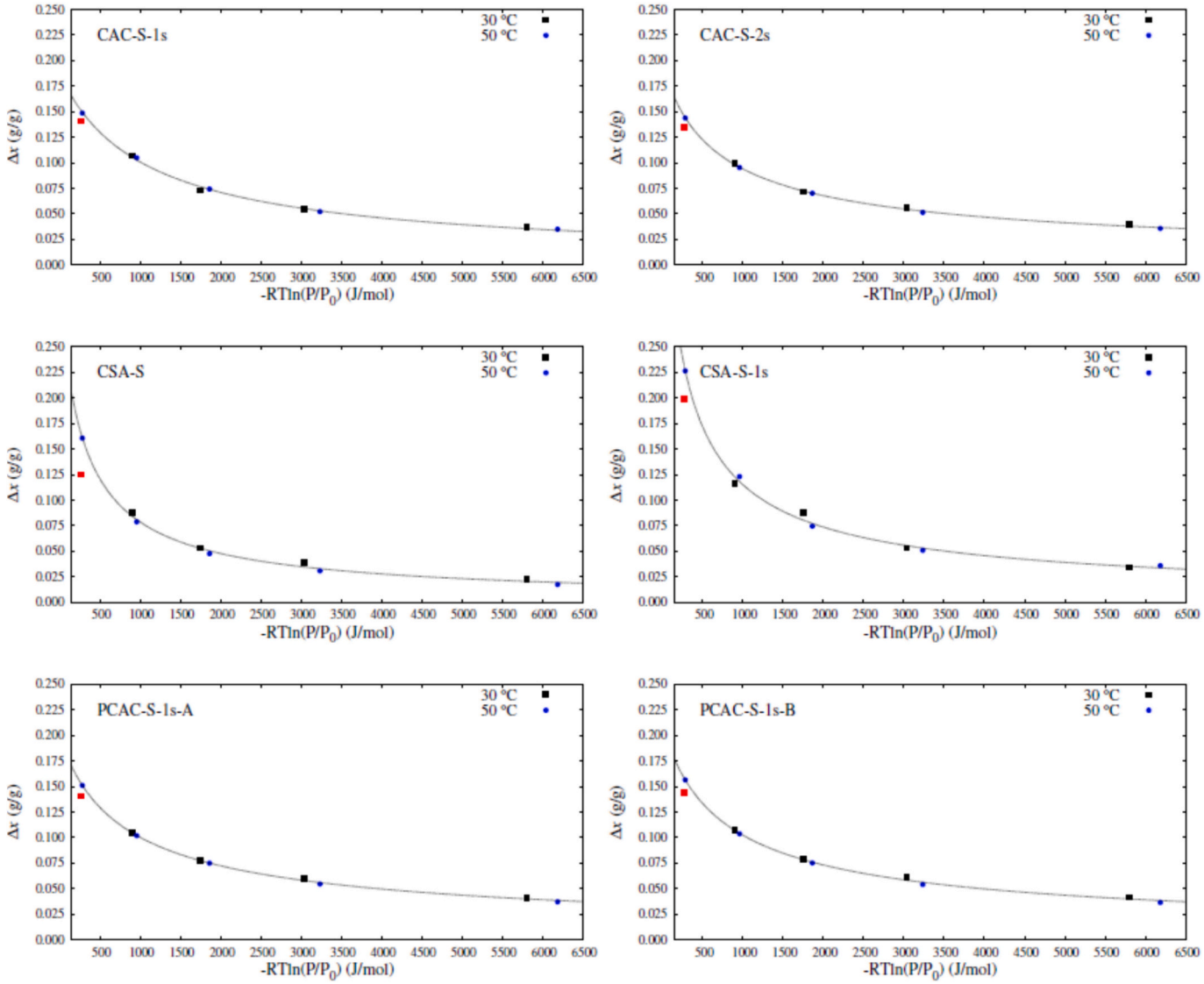

Fig. 4. Adsorbed load (Δx, in g/g) as a function of the adsorption potential defined in Eq. (3). Squares and circles refer to data from the 30 °C-isotherm and 50 °C-isotherm, respectively. All the data are collected in Table S3. See the text for the explanation behind the red square. (For interpretation of the references to colour in this figure legend, the reader is referred to the web version of this article.)

those collected at 30 °C and 90 %rh for the abovementioned reasons. As explained, by sampling the "characteristic curve" at the given potentials linked to the desired temperature, one can virtually obtain any desired adsorption isotherm. To do this, a 3-parameters fitting model has been proposed, namely

$$f(A_{Dub}) = \frac{a}{(A_{Dub} + b)^c} \tag{6}$$

and applied to all the experimental data of each sample, only disregarding outliers collected at 30 °C and 90 %rh. The results of such best-fitting procedure, performed again with a NLLS Levenberg-Marquardt algorithm, are reported in Table 2.

As already mentioned, since the adsorption potential A_{Dub} is itself a function of the thermodynamics variables T and p, the explicit expression of Eq. (6)

$$\Delta x = \frac{a}{[RT\ln(p_0/p) + b]^c}$$

suggests that, by fixing the value of T and substituting the corresponding value of saturation pressure p_0, it is possible to predict all the experimental isotherms. Fig. 5 reports, together with the experimental data, a set of 5 different isotherms corresponding to 10 °C, 30 °C, 50 °C, 70 °C and 90 °C, for all the 6 investigated samples.

These isotherms are necessary in order to derive the corresponding isosteric curves in the Clapeyron charts, thus playing a key role in the assessment of the main thermal and energy figures of merit of the synthesized samples, namely the cycled heat (Q_u) and the energy density (E_d). The relationship between temperature and adsorption pressure is provided by the popular Clausius-Clapeyron via the following estimate of the isosteric heat, q_{is}:

$$q_{is} = R\left(\frac{\partial ln(P)}{\partial\left(-\frac{1}{T}\right)}\right)_x \tag{7}$$

In order to define the thermodynamic cycle, it is important to specify all the relevant operating conditions in which the charging/discharging thermodynamic cycle takes place. Here are the most important properties to be specified:

- T_W, the average winter temperature, that in this case has been chosen to be 10 °C.
- T_S, the average summer hot temperature, which in this case has been estimated to be 30 °C.
- T_A, the user operating temperature, which here is supposed to be 40 °C (this corresponds to a floor heating system).
- T_C, the heat source temperature, equal to 150 °C as concentrated solar has been chosen as heat source.

The cycled heat Q_u of the system, namely the heat that this can deliver per unit of mass of the dry adsorbent after a complete energy storage cycle, can be defined as:

$$Q_u = \frac{q_{is}\Delta\overline{x}}{MM_{H_2O}} \tag{8}$$

where MM_{H_2O} is the water molecular mass, namely 18.015 g/mol, and $\Delta\overline{x}$ is the water uptake achievable by the given cycle, typically much smaller than the maximum water uptake of the material.

It is important to underline that the coordinates $(T^{-1}, \ln p)$ of points A and C reported in Fig. 6 are defined uniquely by the operational thermal boundaries. Once the coordinates are defined, common values of $A_{Dub}(T_A, P_A) = 4670.7$ kJ/mol and $A_{Dub}(T_C, P_C) = 16{,}604.6$ kJ/mol for all the 6 investigated composites are fixed. These values, matched with the "characteristic curve" reported in Fig. 4, provide different amounts of water uptake Δx for each sample. Such values of water uptakes are reported in Fig. 6 and Table 3. Moreover, it is worth stressing that - since the relationship among temperature and pressure is hindered by the saturation vapor pressure of water - the isosteric heat q_{is} as defined in Eq. (7) is equal to 59.84 kJ/mol. Keeping Δx constant means, indeed, that also A_{Dub} is fixed and, according to its definition reported in Eq. (3), temperature and pressure have to vary accordingly and uniquely. The latter value has been obtained through a linear regression in the Clapeyron charts of 5 different pairs of temperature and pressure providing the same $A_{Dub}(T_C, P_C)$. Ultimately, the energy density (E_d) of the material in the given system can be simply derived by multiplying the cycled heat (Q_u) by the dried density of the composites, $d_{140°C}$. Table 3 collects, among the others, the cycled heat and the energy density for the 6 studied composites. As can be observed, the lowest value of Q_u belongs to composite CSA-S, namely the unloaded CSA cement with 70 % of sepiolite and water-to-cement ratio equal to 1.5. This result is in line with what expected as in this sample the salt hydrate $MgSO_4$, main responsible of the thermochemical storage phenomenon, is totally absent.

Moreover, if compared with the result shown by sample CSA-S-1s, that differs from sample CSA-S only for the presence of a 21.5 % in weight of salt, the key role of $MgSO_4$ is evident as it provides an increment on the cycled heat performance >50 %. The highest value of cycled heat is that of sample CAC-S-1s, namely the in situ CAC with 70 % of sepiolite and $w/c = 1.5$, followed by samples PCAC-S-1s-B and PCAC-S-1s-A, respectively. However, these latter samples, the two that have been prepared by mixing CAC and PC in different proportions, do not dissolve if they come into contact with liquid water, unlike sample CAC-S-1s. This aspect might play a key role in the selection criterion for technological purposes of the composite as some condensation phenomena may occur within the device and, if not water resistant, it may undergo a performance decay.

Finally, it is worth underlining that in a previous study (Burlon), cyclability was found to be very high without a significant loss of performance for this kind of composite materials.

5. Preliminary cost analysis

The last step for the suitability evaluation of the developed materials needs to be on their potential economic feasibility in terms of costs of the installed storage capacity. On this regard the *key performance indicator* (KPI) used as a figure of merit and expressed in terms of monetary units per energy storage capacity, namely €/ton, is defined as the ratio between the price of the raw materials, C in €/ton, and the cycled heat, Q_u in kWh/ton. It may be useful to recall that

Table 2
Fitting parameters a, b and c of the experimental data reported in Table S3 through Eq. (6).

Fitting parameters	Sample					
	CSA-S	CSA-S-1s	CAC-S-1s	CAC-S-2s	PCAC-S-1s-A	PCAC-S-1s-B
a (J/mol)	34.46	20.31	50.70	8.32	11.37	12.46
b (J/mol)	262.14	187.20	890.45	435.93	526.95	505.23
c	0.852	0.731	0.824	0.618	0.645	0.656
R^2	0.916	0.930	0.991	0.991	0.988	0.984

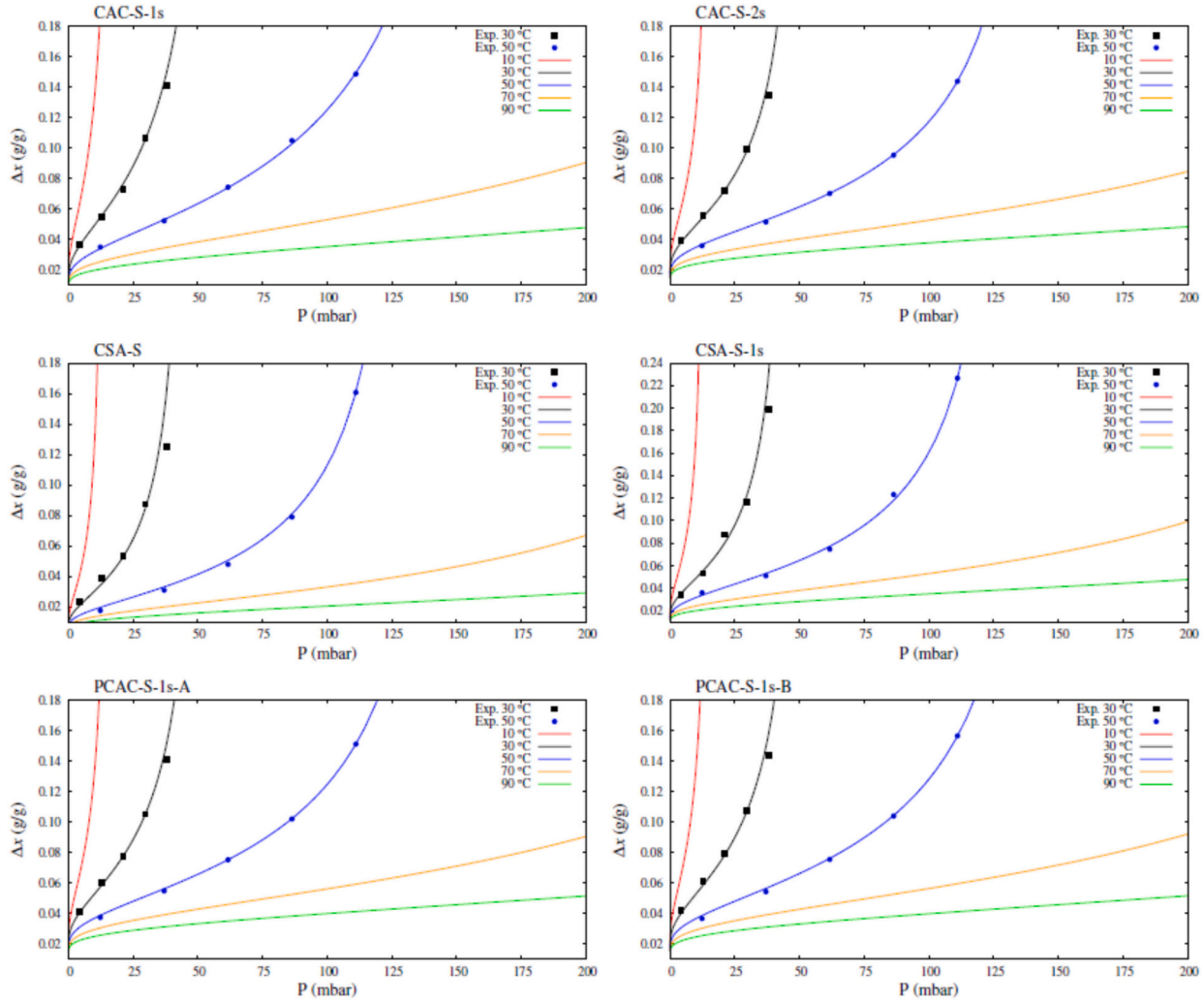

Fig. 5. Predicted isotherms for 5 different temperatures, namely 10 °C, 30 °C, 50 °C, 70 °C and 90 °C for all the 6 investigated samples. As a comparison, experimental 30 °C-data and 50 °C-data are reported as well.

$$1 \bullet \frac{\text{kJ}}{\text{kg}} = \frac{1}{3.6} \bullet \frac{\text{kWh}}{\text{ton}}$$

In order to evaluate C, namely the costs of the only raw materials and neglecting that of labor, processes, components and so on, the following prices were assumed:

- 100 €/ton for PC, even if it is very country dependent [37];
- 400 €/ton for CAC [38];
- 300 €/ton for CSA cement [39];
- 100 €/ton for sepiolite [40];
- 160 €/ton for anhydrous magnesium sulfate [8].

The cost per tons of each composite can be calculated by considering the amount of its constituent materials reported in Table 1, by dividing it by the cycled heat the KPI can be found. Table 4 collects the cycled heat (Q_u) obtained for the CSPM materials (sample CSA-S is thus neglected) together with the total mass of the produced samples (M_{tot}), the cost per ton (C) and the KPI. In order to ease the readability of Table 4, it may be useful to recall that

- CAC-S-1s → CAC, 70 % of sepiolite, $w/c = 1.5$, in situ procedure.
- CAC-S-2s → CAC, 70 % of sepiolite pre-impregnated with H_2O, $w/c = 1.5$, 2-step procedure.
- CSA-S-1s → CSA, 70 % of sepiolite, $w/c = 1.5$, in situ procedure.
- PCAC-S-1s-A → CAC (85 %)-PC (15 %), 70 % of Sep., $w/c = 1.5$, in situ procedure.
- PCAC-S-1s-B → CAC (77.5 %)-PC (22.5 %), 70 % of Sep., $w/c = 1.5$, in situ procedure.

As can be observed, sample CAC-S-2s provides a KPI way too big with respect to the others to be taken into account for a possible use for tackling the TES issues. The remaining samples however show KPI values more or less in line one to the other. It is interesting to notice that despite sample CAC-S-1s shows a higher value of cycled heat Q_u with respect to that of the others, the high cost of CAC has an impact on the KPI value. The presence of a fraction of the cheaper PC in samples PCAC-S-1s-A and PCAC-S-1s-B not only allows to partially compensate this latter aspect, but also provides water resistance to both the composites, a feature that is absent in all the others in-situ samples. Finally, after the characterization of these samples is concluded, it is important to compare the results provided by the synthesized composites materials with those already available in TES literature and also collected in Table 5. As can be observed in Table 5, the samples produced in this work perform better than zeolite 13×/$MgSO_4$ and silica gel/$CaCl_2$, but at the same time are quite far from other systems, in particular those based on the hydration of calcium or lithium chloride. Notice, however, that the amount of saline 'active phase' in the latter systems is 3 times larger than that in the samples here synthesized, but their operation temperature T_C is much lower.

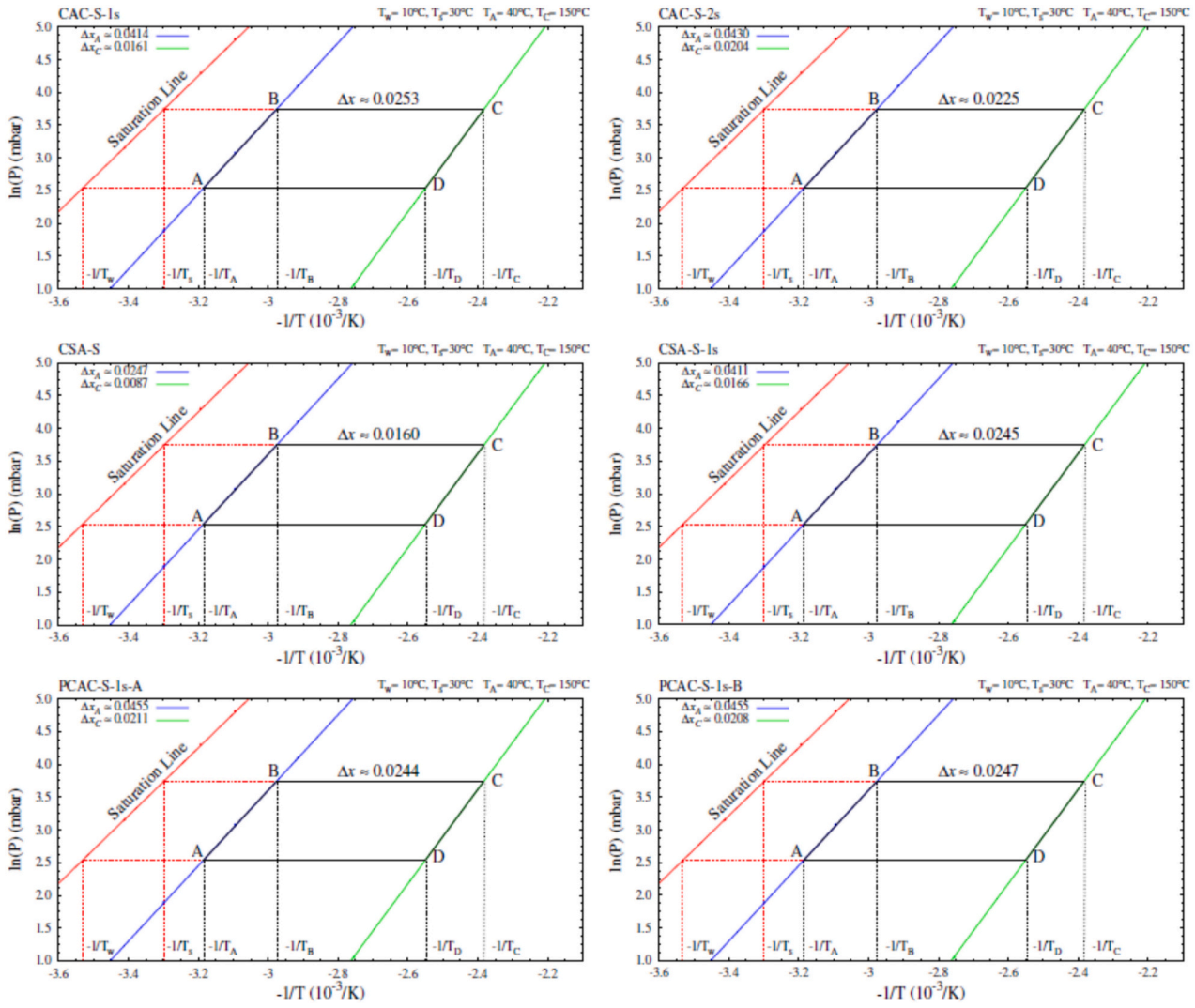

Fig. 6. Charging/discharging thermodynamic cycle for the 6 investigated samples. The operational boundaries in which the cycle takes place are $T_W = 10$ °C, $T_S = 30$ °C, $T_A = 40$ °C, and $T_C = 150$ °C.

Table 3
Water uptakes (Δx) for the points A and C reported in Fig. 5, adsorption load ($\Delta\bar{x}$) for the cycle, dried density ($p_{140°C}$), cycled heat (Q_u) and energy density (E_d) for the 6 studied composites. The E_d values obtained from the preliminary thermal test are reported as a comparison.

	Units	Sample					
		CSA-S	CSA-S-1s	CAC-S-1s	CAC-S-2s	PCAC-S-1s-A	PCAC-S-1s-B
Δx ($A_{Dub}(T_A,P_A)$)	g/g	0.025	0.041	0.041	0.043	0.046	0.046
Δx ($A_{Dub}(T_C,P_C)$)	g/g	0.009	0.017	0.016	0.020	0.021	0.021
$\Delta\bar{x}$	g/g	0.016	0.025	0.025	0.023	0.024	0.025
$d_{140\ °C}$	g/cm^3	0.91	1.03	1.13	0.87	1.05	1.03
Q_u	kJ/kg	53.15	81.41	84.14	74.85	81.17	82.18
E_d	MJ/m^3	48.37	83.85	95.08	65.12	85.23	84.65
$\overline{E_{d(prel.)}}$	MJ/m^3	66.42	110.33	102.04	–	94.25	84.52

6. Conclusion

The aim of this work was to synthesize and thermally characterize cement-based composite salt inside porous matrix (CSPM) materials for thermochemical energy storage (TES). Following the path outlined over the years by the research group, three different cement families have been investigated: the most popular Portland cement (PC), calcium aluminate cement (CAC) and calcium sulfoaluminate (CSA) cement. A significant quantity of sepiolite, up to 70 % concerning the mass of cement powder, has been investigated as an addition to the cement matrix to reduce costs and enhance porosity. The new in-situ synthesis technique, especially suitable for cements, offered advantages such as simplicity, speed, and reproducibility, enabling better control of salt content and higher quantities of the 'active phase' in the composite.

Six selected samples underwent water sorption analysis at 30 °C and 50 °C, followed by assessment of storage capabilities using Clapeyron charts and defined operational boundaries to derive key thermal characterization quantities, namely the isosteric heat, the water uptake and thus both the cycled heat and energy density. To do this, the Polanyi adsorption potential theory has been applied to obtain other isotherms

Table 4
Cycled heat (Q_u, in kWh/ton), total mass of the samples produced (M_{tot}, in g), production cost (C, in €/ton) and KPI (in €/kWh) for the 5 samples containing salt hydrates.

Sample	Q_u (kWh/ton)	M_{tot} (g)	C (€/ton)	KPI (€/kWh)
CAC-S-1s	23.37	156.69	233.3	10.0
CAC-S-2s	20.79	111.99	327.5	15.8
CSA-S-1s	22.61	140.07	212.4	9.4
PCAC-S-1s-A	22.55	152.77	222.0	9.9
PCAC-S-1s-B	22.83	152.48	212.4	9.3

Table 5
Comparison of the best composites developed with other materials in literature. The KPI column shows the values in terms of raw materials' costs variations.

Material	Salt (%)	T_C (°C)	E_d (GJ/ton)	C (€/ton)	KPI (€/kWh)	Ref.
CAC, 70 % sep., w/c = 1.5	21.4	150	0.096	233.3	10.0	This work sample CAC-S-1s
CSA, 70 % sep., w/c = 1.5	21.5	150	0.084	212.4	9.4	This work sample CSA-S-1s
CAC(85 %)-PC (15 %), 70 % sep., w/c = 1.5	21.8	150	0.085	222.0	9.9	This work sample PCAC-S-1s-A
CAC(77.5 %)-PC (22.5 %), 70 % sep., w/c = 1.5	21.5	150	0.084	212.4	9.3	This work sample PCAC-S-1s-B
PC/$MgSO_4$	21	80	0.078	132.6	3.9–6.1	[29]
		140	0.18		1.7–2.7	
Vermiculite/$CaCl_2$	57.3	85	1.00	329	1.18	[41]
vermiculite/LiCl	59	85	2.6	4761	6.59	[42]
Zeolite 13×	–	180	0.54	2000	13.4	[4]
	–	160	0.38		18.5	
Zeolite 13×/$MgSO_4$	10–25	150	0.65	1805	10.03	[4]
Silica Gel/$CaCl_2$	33.7	90	0.58	3483.5	26.39	[4]

from the available data. Finally, a preliminary cost analysis contextualized the composites in terms of €/kWh within the energy market.

The key performance indicators of the best results have shown that the obtained composites are interesting but not a breakthrough in TES technology. The best result is obtained by the sample PCAC-S-1s-B, that is the sample made of calcium aluminate cement with the addition of 22.5 % of Portland cement and sepiolite, obtained by the in-situ preparation method. This sample shows a cycled heat of 22.83 kWh/ton, an energy density of 0.084 GJ/ton, a cost of 212.4 €/ton and a KPI of 9.3 €/kWh. This KPI value is superior to that of highly performing materials such as Zeolite 13×, Zeolite 13×/$MgSO_4$ or silica gel/$CaCl_2$. However it falls short of the KPI demonstrated by vermiculite/$CaCl_2$, vermiculite/LiCl and Portland cement with $MgSO_4$. On the other hand, vermiculite-based materials can exhibit deliquescence or mass transport issues [24] while Portland cement could have issues related to presence of sulfates, that could modify long-term performance. A positive aspect of these novel calcium aluminate and sulfo-aluminate cement-based composites is that their cost is significantly lower than that of the majority of the other composites found in the literature, so that an optimization of support porosity and salt dispersion could provide a further improvement in performance and thus in KPI. The focus on cement-based materials is indeed related to their easy and widespread availability and to their low cost. With respect to Portland cement explored in previous articles, calcium aluminate and sulfo-aluminate cements have a shorter history, a narrower field of application and consequently higher costs, so there is the possibility of reducing the costs of CAC and CSA cements by scale economies. The mixture of CAC with PC is also interesting, since not only stabilizes the produced material with respect of liquid water, but also reduces the costs still maintaining high resistance to sulfates.

Finally, it's important to note that this study focused solely on material-based energy density for comparative analysis. For real engineering applications, the energy density has to be computed including also the volume of the other plant items. In this respect, according to [9], only moving from bulk material to the sorption bed, for an open system, the energy density decreases by approximately 30 %, while for a closed system, the expected reduction is around 50 %.

CRediT authorship contribution statement

Simone Salustro: Writing – review & editing, Writing – original draft, Visualization, Validation, Software, Methodology, Formal analysis, Data curation. **Luca Lavagna:** Writing – review & editing, Writing – original draft, Validation, Investigation, Data curation, Conceptualization. **Vito Fernicola:** Writing – review & editing, Validation, Supervision, Methodology. **Denis Smorgon:** Writing – review & editing, Validation, Methodology, Investigation. **Alessio Mondello:** Writing – review & editing, Visualization, Validation, Software. **Eliodoro Chiavazzo:** Writing – review & editing, Supervision, Resources, Project administration, Funding acquisition, Conceptualization. **Matteo Pavese:** Writing – review & editing, Supervision, Resources, Project administration, Conceptualization.

Declaration of competing interest

The authors declare that they have no known competing financial interests or personal relationships that could have appeared to influence the work reported in this paper.

Data availability

Data will be made available on request.

Acknowledgement

We acknowledge financial support from:
PNRR - M4C2 - AVVISO 341/2022 - NEST - PE00000021 CUP - E13C22001890001 SPOKE 6 - Energy Storage.
Funded by EU via Next Generation EU, M4C2, investment 1.1 (project: PRIN PNRR 2022 “LObSTER”, N. P2022EERT9).

Appendix A. Supplementary data

Supplementary data to this article can be found online at https://doi.org/10.1016/j.est.2024.112308.

References

[1] V. Palomba, A. Frazzica, Recent advancements in sorption technology for solar thermal energy storage applications, Sol. Energy 192 (2019) 69–105, https://doi.org/10.1016/j.solener.2018.06.102.
[2] J.W. McBain, XCIX., The mechanism of the adsorption (“sorption”) of hydrogen by carbon, Lond. Edinb. Dublin Philos. Mag. J. Sci. 18 (1909) 916–935, https://doi.org/10.1080/14786441208636769.
[3] Y. Zhang, R. Wang, Sorption thermal energy storage: concept, process, applications and perspectives, Energy Storage Mater. 27 (2020) 352–369, https://doi.org/10.1016/j.ensm.2020.02.024.
[4] N. Yu, R.Z. Wang, L.W. Wang, Sorption thermal storage for solar energy, Prog. Energy Combust. Sci. 39 (2013) 489–514, https://doi.org/10.1016/j.pecs.2013.05.004.
[5] L. Hui, N.K. Edem, L.P. Nolwenn, L. Lingai, Evaluation of a seasonal storage system of solar energy for house heating using different absorption couples, Energy Convers. Manag. 52 (2011) 2427–2436, https://doi.org/10.1016/j.enconman.2010.12.049.
[6] S. Vasta, V. Brancato, D. La Rosa, V. Palomba, G. Restuccia, A. Sapienza, A. Frazzica, Adsorption heat storage: state-of-the-art and future perspectives, Nanomaterials 8 (2018), https://doi.org/10.3390/nano8070522.

[7] G. Trezza, L. Bergamasco, M. Fasano, E. Chiavazzo, Minimal crystallographic descriptors of sorption properties in hypothetical MOFs and role in sequential learning optimization, npj Comput. Mater. 8 (2022) 123, https://doi.org/10.1038/s41524-022-00806-7.
[8] F. Trausel, A.-J. de Jong, R. Cuypers, A review on the properties of salt hydrates for thermochemical storage, Proc. 2nd Int. Conf. Sol. Heat. Cool. Build. Ind. SHC 2013 (48) (2014) 447–452, https://doi.org/10.1016/j.egypro.2014.02.053.
[9] P.A.J. Donkers, L.C. Sögütoglu, H.P. Huinink, H.R. Fischer, O.C.G. Adan, A review of salt hydrates for seasonal heat storage in domestic applications, Appl. Energy 199 (2017) 45–68, https://doi.org/10.1016/j.apenergy.2017.04.080.
[10] M. Richter, E.-M. Habermann, E. Siebecke, M. Linder, A systematic screening of salt hydrates as materials for a thermochemical heat transformer, Thermochim. Acta 659 (2018) 136–150, https://doi.org/10.1016/j.tca.2017.06.011.
[11] Y.I. Aristov, G. Restuccia, G. Cacciola, V.N. Parmon, A family of new working materials for solid sorption air conditioning systems, Appl. Therm. Eng. 22 (2002) 191–204, https://doi.org/10.1016/S1359-4311(01)00072-2.
[12] Y.I. Aristov, Novel materials for adsorptive heat pumping and storage: screening and nanotailoring of sorption properties, J. Chem. Eng. Jpn 40 (2007) 1242–1251, https://doi.org/10.1252/jcej.07WE228.
[13] V. Brancato, L. Gordeeva, A. Sapienza, V. Palomba, S. Vasta, A. Grekova, A. Frazzica, Y. Aristov, Experimental characterization of the LiCl/Vermiculite composite for sorption heat storage applications, Int. J. Refrig. (2018), https://doi.org/10.1016/j.ijrefrig.2018.08.006.
[14] A. Grekova, L. Gordeeva, Y. Aristov, Composite sorbents "Li/Ca halogenides inside multi-wall carbon nano-tubes" for thermal energy storage, Sol. Energy Mater. Sol. Cells 155 (2016) 176–183, https://doi.org/10.1016/j.solmat.2016.06.006.
[15] D. Mohapatra, J. Nandanavanam, Salt in matrix for thermochemical energy storage - a review, Int. Conf. Novel Mater. Technol. Energy Environ. Appl. 72 (2023) 27–33, https://doi.org/10.1016/j.matpr.2022.05.453.
[16] M.H. Nguyen, M. Zbair, P. Dutournié, S. Bennici, Thermochemical sorption heat storage: investigate the heat released from activated carbon beads used as porous host matrix for MgSO4 salt, J. Energy Storage 59 (2023) 106452, https://doi.org/10.1016/j.est.2022.106452.
[17] S. Hongois, F. Kuznik, P. Stevens, J.-J. Roux, Development and characterisation of a new MgSO4−zeolite composite for long-term thermal energy storage, Sol. Energy Mater. Sol. Cells 95 (2011) 1831–1837, https://doi.org/10.1016/j.solmat.2011.01.050.
[18] A. Fopah Lele, K. Korhammer, N. Wegscheider, H.U. Rammelberg, T. Osterland, W. Ruck, Thermal Conductivity Measurement of Salt Hydrate as Porous Material Using Calorimetric (DSC) Method, 2013, https://doi.org/10.13140/RG.2.1.3034.9927.
[19] S.P. Casey, J. Elvins, S. Riffat, A. Robinson, Salt impregnated desiccant matrices for 'open' thermochemical energy storage—selection, synthesis and characterisation of candidate materials, Energ. Buildings 84 (2014) 412–425, https://doi.org/10.1016/j.enbuild.2014.08.028.
[20] M.-M. Druske, A. Fopah-Lele, K. Korhammer, H.U. Rammelberg, N. Wegscheider, W. Ruck, T. Schmidt, Developed materials for thermal energy storage: synthesis and characterization, Int. Conf. Appl. Energy ICAE2014 61 (2014) 96–99, https://doi.org/10.1016/j.egypro.2014.11.915.
[21] B. Yilmaz, B. Yüksel, G. Orhan, D. Aydin, Z. Utlu, Synthesis and characterization of salt-impregnated anodic aluminum oxide composites for low-grade heat storage, Int. J. Miner. Metall. Mater. 27 (2020) 112–118, https://doi.org/10.1007/s12613-019-1890-x.
[22] H. Jarimi, A. Devrim, Y. Zhang, Y. Ding, O. Ramadan, X. Chen, A. Dodo, Z. Utlu, S. Riffat, Materials characterization of innovative composite materials for solar-driven thermochemical heat storage (THS) suitable for building application, Int. J. Low-Carbon Technol. 14 (2019) 313–325, https://doi.org/10.1093/ijlct/ctx017.
[23] P. D'Ans, E. Courbon, A. Permyakova, F. Nouar, C. Simonnet-Jégat, F. Bourdreux, L. Malet, C. Serre, M. Frère, N. Steunou, A new strontium bromide MOF composite with improved performance for solar energy storage application, J. Energy Storage 25 (2019) 100881, https://doi.org/10.1016/j.est.2019.100881.
[24] L. Aghemo, L. Lavagna, E. Chiavazzo, M. Pavese, Comparison of key performance indicators of sorbent materials for thermal energy storage with an economic focus, Energy Storage Mater. 55 (2023) 130–153, https://doi.org/10.1016/j.ensm.2022.11.042.
[25] W. Hua, H. Yan, X. Zhang, X. Xu, L. Zhang, Y. Shi, Review of salt hydrates-based thermochemical adsorption thermal storage technologies, J. Energy Storage 56 (2022) 106158, https://doi.org/10.1016/j.est.2022.106158.
[26] J. Lin, Q. Zhao, H. Huang, H. Mao, Y. Liu, Y. Xiao, Applications of low-temperature thermochemical energy storage systems for salt hydrates based on material classification: a review, Sol. Energy 214 (2021) 149–178, https://doi.org/10.1016/j.solener.2020.11.055.
[27] A.Hauer, Thermal energy storage with zeolite for heating and cooling applications, ZAE Bayern Cent. Appl. Energy Res. Domagkstr11 (n.d.).
[28] H. Wu, P. Trens, B. Fraisse, F. Salles, J. Zajac, Hydration mechanism in Ce-exchanged zeolites and heat release performances upon adsorption of water vapour in support of their potential use in thermochemical storage of energy under mild conditions of adsorbent regeneration and saturation, Microporous Mesoporous Mater. 296 (2020) 109999, https://doi.org/10.1016/j.micromeso.2020.109999.
[29] L. Lavagna, D. Burlon, R. Nisticò, V. Brancato, A. Frazzica, M. Pavese, E. Chiavazzo, Cementitious composite materials for thermal energy storage applications: a preliminary characterization and theoretical analysis, Sci. Rep. 10 (2020) 12833, https://doi.org/10.1038/s41598-020-69502-0.
[30] L. Lavagna, R. Nisticò, An insight into the chemistry of cement—a review, Appl. Sci. 13 (2022) 203, https://doi.org/10.3390/app13010203.
[31] M. Thommes, K. Kaneko, A.V. Neimark, J.P. Olivier, F. Rodriguez-Reinoso, J. Rouquerol, K.S.W. Sing, Physisorption of gases, with special reference to the evaluation of surface area and pore size distribution (IUPAC technical report), Pure Appl. Chem. 87 (2015) 1051–1069, https://doi.org/10.1515/pac-2014-1117.
[32] S. Brunauer, P.H. Emmett, E. Teller, Adsorption of gases in multimolecular layers, J. Am. Chem. Soc. 60 (1938) 309–319, https://doi.org/10.1021/ja01269a023.
[33] S. Lowell, J. Shields, M. Thomas, M. Thommes, Characterization of porous solids and powders: surface area, Pore Size Dens. (2006), https://doi.org/10.1007/978-1-4020-2303-3.
[34] Y.I. Aristov, Adsorptive transformation of heat: principles of construction of adsorbents database, Appl. Therm. Eng. 42 (2012) 18–24, https://doi.org/10.1016/j.applthermaleng.2011.02.024.
[35] N.D. Hutson, R.T. Yang, Theoretical basis for the Dubinin-Radushkevitch (D-R) adsorption isotherm equation, Adsorption 3 (1997) 189–195, https://doi.org/10.1007/BF01650130.
[36] M. Steiger, K. Linnow, H. Juling, G. Gülker, A.E. Jarad, S. Brüggerhoff, D. Kirchner, Hydration of $MgSO_4 \cdot H_2O$ and generation of stress in porous materials, Cryst. Growth Des. 8 (2008) 336–343, https://doi.org/10.1021/cg060688c.
[37] Europäische Kommission (Ed.), Competitiveness of the European Cement and Lime Sectors: Final Report, Publications Office of the European Union, Luxembourg, 2018.
[38] P. Hewlett, Lea's Chemistry of Cement and Concrete, Elsevier Science, 2003.
[39] M.A.G. Aranda, A.G. De la Torre, 18 - Sulfoaluminate cement, in: F. Pacheco-Torgal, S. Jalali, J. Labrincha, V.M. John (Eds.), Eco-Effic. Concr, Woodhead Publishing, 2013, pp. 488–522, https://doi.org/10.1533/9780857098993.4.488.
[40] N. Song, A. Hursthouse, I. McLellan, Z. Wang, Treatment of environmental contamination using sepiolite: current approaches and future potential, Environ. Geochem. Health 43 (2021) 2679–2697, https://doi.org/10.1007/s10653-020-00705-0.
[41] Yu.I. Aristov, M.M. Tokarev, G. Cacciola, G. Restuccia, Selective water sorbents for multiple applications, 1. CaCl2 confined in mesopores of silica gel: sorption properties, React. Kinet. Catal. Lett. 59 (1996) 325–333, https://doi.org/10.1007/BF02068130.
[42] A.D. Grekova, L.G. Gordeeva, Y.I. Aristov, Composite "LiCl/vermiculite" as advanced water sorbent for thermal energy storage, Appl. Therm. Eng. 124 (2017) 1401–1408, https://doi.org/10.1016/j.applthermaleng.2017.06.122.